

# Statistical Models of Nuclear Fragmentation

Scott Pratt and Subal Das Gupta\*  
*Department of Physics and Astronomy and  
National Superconducting Cyclotron Laboratory,  
Michigan State University, East Lansing, MI 48824 USA*  
(November 12, 2018)

A method is presented that allows exact calculations of fragment multiplicity distributions for a canonical ensemble of non-interacting clusters. Fragmentation properties are shown to depend on only a few parameters. Fragments are shown to be copiously produced above the transition temperature. At this transition temperature, the calculated multiplicity distributions broaden and become strongly super-Poissonian. This behavior is compared to predictions from a percolation model. A corresponding microcanonical formalism is also presented.

## I. INTRODUCTION

Heavy ion collisions where excitation energies are of the order of 10 MeV per nucleon probe the energy regime where the nuclear liquid gas transition is expected to take place. Below energies of approximately  $50A$  MeV, symmetric collisions are expected to produce sources that evaporate particles as would be expected from a hot liquid drop, whereas above this threshold, the excited source is expected to explode, producing larger clusters through simultaneous multi-fragmentation. In this energy regime, the process of fragment production is not clear, and comparisons with data have been made with a disparate set of models, ranging in simplicity from percolation descriptions [1,2] and lattice gas models [3], to evaporative models [4], dynamical simulations [6,8,7,9,10], and microcanonical samplings [11,12].

Fluctuations behave in a special manner in the region of phase transition, so it should seem that the study of fluctuations of fragmentation observables might prove insightful for investigating multifragmentation. Moretto and collaborators [13] have measured multiplicity distributions of intermediate-mass fragments (IMFs) as a function of excitation energy for a variety of projectile/target combinations utilizing beams with energies up to  $60 A$  MeV. The analysis showed sub-Poissonian multiplicity distributions that could accurately be described with binomial distributions. These observations have inspired a variety of explanations [14–17].

Recently, Chase and Mekjian [18] have discovered a method for exact calculation of the canonical partition function for non-interacting clusters. In this paper we extend this approach to include fragmentation observables. We present a method for exact determination of both multiplicity distributions and their moments. When raising the temperature while keeping the volume fixed, we observe a sharp transition for fragmentation at the same point where the specific heat peaks. At this threshold, the multiplicity distribution becomes remarkably wide. We associate this behavior with a first order phase transition and remark that the broadening might well disappear in a microcanonical treatment.

We parameterize the width of the fragment multiplicity distribution, relative to the mean, with a correlation coefficient  $\xi$  which is described in the next section. The method for calculating fragmentation observables from a canonical ensemble is presented in section III while the results are presented in section IV. In section V we contrast the results of this model with those of a percolation model. Expressions that could be used for microcanonical calculations are presented in section VI.

## II. MULTIPLICITY DISTRIBUTIONS AND THE CORRELATION COEFFICIENT

A super or sub-Poissonian multiplicity distribution is one whose variance exceeds or falls below its mean respectively. The difference of the variance and the mean can also be written as a correlation. We demonstrate this by considering the emission into an arbitrarily large number of states  $i$ , each of which is infinitesimally probable. A state could be defined as a specific type of IMF emitted into an arbitrarily small bin in momentum space. The difference of the variance and the mean is

---

\*Permanent address: Physics Department, McGill University, Montreal, Quebec, Canada, H3A 2T8

$$\begin{aligned}
\sigma^2 - \langle n \rangle &= \sum_{i,j} (\langle n_i - \langle n_i \rangle \rangle \langle n_j - \langle n_j \rangle \rangle) - \sum_i \langle n_i \rangle \\
&= \sum_{i \neq j} (\langle n_i - \langle n_i \rangle \rangle \langle n_j - \langle n_j \rangle \rangle) + \sum_i (\langle n_i - \langle n_i \rangle \rangle^2 - \langle n_i \rangle)
\end{aligned} \tag{1}$$

If the bins are arbitrarily small, one may discard the terms in the second sum proportional to  $\langle n_i \rangle^2$ , then use the fact that  $n_i^2 = n_i$  for  $n_i=0$  or  $1$ , to discard the remainder of the second term and obtain,

$$\xi \equiv \frac{\sigma^2 - \langle n \rangle}{\langle n \rangle^2} = \frac{\sum_{i \neq j} (\langle n_i - \langle n_i \rangle \rangle \langle n_j - \langle n_j \rangle \rangle)}{\langle n \rangle^2} \tag{2}$$

Here,  $\xi$  can be interpreted as a correlation coefficient. It is positive if the emission into two different bins is positively correlated. The only assumption going into this derivation is that the bins may be divided into arbitrarily small sizes.

The simplest examples of sub- and super-Poissonian multiplicity distributions are the binomial and negative binomial distributions. The binomial distribution is defined in terms of two parameters,  $p$  and  $N$ .

$$P_n = \frac{N!}{n!(N-n)!} p^n (1-p)^{N-n}, \tag{3}$$

where  $p$  is the probability of success in one of  $N$  tries. For the binomial distribution the mean and correlation coefficients become

$$\langle n \rangle_{\text{bin.}} = pN \tag{4}$$

$$\xi_{\text{bin.}} = -1/N, \tag{5}$$

and stays negative. Like most correlations it is proportion to the inverse of the system size.

The negative binomial distribution is also defined by two parameters  $p$  and  $N$ .

$$P_n = \frac{(N+n-1)!}{(N-1)!n!} \frac{p^n}{(1+p)^{N+n}}. \tag{6}$$

The correlation coefficient in this case is opposite to that of the binomial distribution.

$$\langle n \rangle_{\text{neg.bin.}} = pN \tag{7}$$

$$\xi_{\text{neg.bin.}} = 1/N. \tag{8}$$

Binomial and negative binomial distributions result when one considers populating  $N$  quantum levels with fermions or bosons respectively with  $p$  representing the average population of each level.

Random emission from a large number of uncorrelated sources leads to a Poissonian distribution. The binomial distribution suggests that conservation of particle number would give a negative correlation coefficient of order  $1/N$ , where  $N = A/a$  is the number of IMFs of characteristic size  $a$  that could fit into the system. For sufficiently small systems, this negative contribution from particle-number conservation dominates, with the extreme case being where  $a$  is more than half the system size meaning that no more than one IMF can be emitted. Other negative correlations are expected due to energy conservation. If IMF emission requires energy, e.g. escaping a Coulomb barrier, energy conservation is expected to reduce the probability of emitting a second IMF. We will see in the next sections that positive correlations can arise, principally due to surface considerations.

Aside from the size of the correlations, it is also of interest to understand whether the entire multiplicity distribution, is well described by a two-parameter fit to a binomial or negative binomial distribution. If the reduction of the results to two parameters is valid, comparison of different models and data is greatly simplified.

### III. CANONICAL DISTRIBUTIONS OF NON-INTERACTING CLUSTERS

Chase and Mekjian have shown that canonical partition functions can be easily calculated in terms of the partition functions of single clusters. This allows the calculation of thermodynamic quantities for a system of fixed nucleon number without resorting to numerically intensive Monte-Carlo procedures. If the partition function for a single cluster of size  $a_k$  is denoted by  $\omega_k$ , the partition function for a system of size  $A$  may be written,

$$\begin{aligned}\Omega_A &\equiv \sum_{\langle \sum n_k a_k = A \rangle} \prod_k \frac{\omega_k^{n_k}}{n_k!} \\ &= \sum_k \omega_k \frac{k}{A} \Omega_{A-a_k}\end{aligned}\quad (9)$$

Thus,  $\Omega_A$  is expressed recursively in terms of  $\omega_k$  and  $\Omega_{A'}$  for  $A' < A$ . Proof of this relation is given in the appendix. The only shortcoming of this approach is that explicit (not mean field) interactions between fragments are ignored.

Moments of the multiplicity distribution may be expressed in terms of the partition functions. The moments can then be used to derive the correlation coefficient,  $\xi_a$  defined in Eq. (2) or the multiplicity distribution as discussed below. The first moment is the mean which is defined as:

$$\langle n_k \rangle = \omega_k \frac{\Omega_{A-a_k}}{\Omega_A} \quad (10)$$

Rather than considering moments,  $\langle n_b^m \rangle$ , it is more convenient to consider factorial moments,  $F_{b,A,m}$ , defined as:

$$F_{b,A,m} \equiv \langle n_b(n_b - 1) \cdots (n_b - m + 1) \rangle \quad (11)$$

Calculation of the factorial moments for  $n_b$  defined in Eq. (11) is simple if  $b$  refers to single species  $k$ :

$$F_{k,A,m} = \omega_k^m \frac{\Omega_{A-ma_k}}{\Omega_A}. \quad (12)$$

However, if  $b$  refers to a set of species,  $n_b = \sum_{k \in b} n_k$ , where the various species that comprise  $b$  have different masses, Eq. (12) is no longer valid. One must then generate the factorial moments using the recursion relation,

$$F_{b,A,m} = \sum_{k \in b} \omega_k F_{b,A-a_k,m-1} \frac{\Omega_{A-a_k}}{\Omega_A}, \quad (13)$$

which is true in general. The proofs of Eq. (12) and Eq. (13) are given in the second section of the appendix.

As shown in the third subsection of the appendix, factorial moments are sufficient for calculating the entire multiplicity distribution via the relation,

$$P_{b,A,n} = \sum_{m \geq n} F_{b,A,m} \frac{1}{(m-n)!n!} (-1)^{m-n}, \quad (14)$$

where  $P_{b,A,n}$  gives the probability of viewing  $n$  fragments of type  $b$  in a system of size  $A$ .

More directly, one may also generate the multiplicity distribution, without knowing the factorial moments, through the recursion relation,

$$P_{b,A,n} = \frac{1}{n} \sum_{k \in b} \omega_k P_{b,A-a_k,n-1} \frac{\Omega_{A-a_k}}{\Omega_A}. \quad (15)$$

Proof of Eq. (15) is presented in the appendix. This direct method of producing the multiplicity distribution has proven more numerically stable than generating the distribution from the factorial moments. This improvement can be traced to the alternating signs in Eq. (14).

Summarizing the technique, one starts by calculating partition functions for individual fragments  $\omega_k$ . One may then generate partition functions,  $\Omega_A$ , by using the recursion relation, Eq. (9). The recursion relation for factorial moments, Eq. (13), then allows one to generate the factorial moments, which in turn allow the determination of the entire multiplicity distribution using Eq. (14). Alternatively, one may calculate the multiplicity distributions directly using Eq. (15). The obtained multiplicity distributions are exact. Although the sums used in the recursion relation are performed numerically, they require only a fraction of a second of computer time.

#### IV. A LIQUID-DROP PICTURE FOR INDIVIDUAL CLUSTERS

For our purposes, we consider the partition function for individual fragments of mass  $k$  as,

$$\omega_k = V \left\{ \frac{a_k M T}{2\pi} \right\}^{3/2} e^{-F_{k,int}/T}, \quad (16)$$

$$F_{k,int} = f_b a_k + f_s a_k^{2/3} + f_c \frac{1}{4} k^{5/3}, \quad (17)$$

where the volume of the system is  $V$ , the mass of a single nucleon is  $M$ , and the fragment's internal free energy  $F_{k,int}$  is split into a bulk term and a surface term. One sees that the bulk term is irrelevant in determining fragmentation observables since it factors out of the partition function. Thus, aside from the system size  $A$ , all fragmentation observables are determined by three parameters, the ratio of the surface term to the temperature  $f_s/T$ , the intrinsic entropy,  $s \equiv (V/A)(MT)^{3/2}$ , and Coulomb term,  $f_c$ . This implies that many details of a system's microscopic makeup, e.g. Fermi vs. Bose nature of the internal excitation, are irrelevant in determining the statistics of fragmentation. If the surface term is negligible fragmentation is determined purely by the intrinsic entropy.

For the surface and Coulomb terms, we use the parameters of the nuclear liquid-drop model,

$$f_s = 17.2 \text{ MeV} \quad (18)$$

$$f_c = 0.70 \left( 1 - \left( \frac{\rho}{\rho_0} \right)^{1/3} \right) \text{ MeV}, \quad (19)$$

where the form of the Coulomb term was taken to account for the screening of the Coulomb repulsion by the nuclear medium in a Wigner-Seitz like parameterization [12] with  $\rho_0$  referring to nuclear saturation density of  $0.15 \text{ fm}^{-3}$ .

All the calculations presented in this paper assumed a density of one third of nuclear matter density. The behavior at different densities is not qualitatively different, with the exception of the relative importance of the Coulomb term. The fragmentation transition described below occurs when  $s = (1/\rho)(mT)^{3/2}$  is of order unity. Therefore a change of density affects the temperature where fragmentation sets in. An excluded volume could easily be incorporated into the problem by replacing  $V$  with  $V(1 - \rho/\rho_0)$ . This is equivalent to changing the density, and does not qualitatively affect the results. The surface energy is chosen to be a constant,  $f_s = 17.2 \text{ MeV}$ . One could imagine scaling  $f_s$  as a function of  $\rho$  or temperature, although one might object to incorporating a temperature dependence that is not of the nature,  $e^{E/T}$ . The choice of  $f_s$  does affect the transition temperature and its width. Larger choices of  $f_s$  lead to sharper transitions. The surface term should disappear at the critical point. Although it is easy to incorporate excluded volume effects and a running surface term, we choose not to, as our principal goal in this study is to understand the general properties of this approach.

In Figure 1, the mass distribution  $dN/da$  is shown for three temperatures,  $T=7.0, 7.8$  and  $8.6 \text{ MeV}$ . The overall size of the system was chosen to be 250 and Coulomb effects were neglected in these calculations. The mass distribution has been multiplied by  $a$  to emphasize how the composite nucleons are partitioned into the various sized drops. At  $7 \text{ MeV}$ , the nucleons are largely contained in one drop, while at the higher temperature, nearly all the particles are part of small clusters.

The average multiplicity of intermediate-mass fragments ( $5 < a \leq 40$ ), denoted as IMFs, are shown in the upper panel of Figure 2 for the cases where the density is  $0.05 \text{ fm}^{-3}$  and the overall system size is again  $A = 100$ . Results are plotted against the temperature, both for the case where the Coulomb term is included as well as for the case where it is neglected. The inclusion of Coulomb pushes fragmentation down towards lower temperatures. The trend would strengthen if we were to consider larger systems. When the excitation energy exceeds the fragmentation threshold, average IMF multiplicities quickly climb to over a half dozen per event.

Correlation coefficients are shown in the lower panel of Figure 2 with the system size is set at 100. Coefficients are shown both for the case where Coulomb is included and for the case where Coulomb is neglected.

When Coulomb is neglected super-Poissonian behavior ensues at lower excitations as evidenced by the positive values of  $\xi$ . At low temperatures, this behavior may be understood by considering the surface penalty for emitting a single fragment of mass  $a$ ,

$$\Gamma(A \rightarrow A - a) \propto \exp \left\{ -a \frac{d}{dA} (F_{\text{surf}}/T) \right\} \quad (20)$$

If a second IMF is emitted, it feels the same penalty, except for the fact that  $dF/dA$  is evaluated at a smaller overall size,  $A - a$ . The correlation thus becomes,

$$\begin{aligned} \xi_{\text{surf}} &\approx \frac{\Gamma(A \rightarrow A - a)\Gamma(A \rightarrow A - a)}{\Gamma(A - a \rightarrow A - 2a)^2} \\ &\approx \frac{a^2}{T} \frac{d^2 F_{\text{surf}}}{dA^2} \end{aligned} \quad (21)$$

$$= \frac{2a^2 f_s}{9T} A^{-4/3}.$$

The dashed line represents the surface contribution to  $\xi$  and closely follows the statistical calculation at lower temperatures. The average size of an IMF was used for  $a$ .

The inclusion of Coulomb reduced  $\xi$  to negative values as seen in Figure 2. The Coulomb contribution to  $\xi$  may be approximated in a similar fashion as the surface contribution,

$$\xi_{\text{coul}} \approx -\frac{5a^2 f_c}{9T} A^{-1/3}. \quad (22)$$

Again, the approximation is plotted as a dashed line in the lower panel of Figure 2.

The simple estimate of  $\xi$  works well at low temperature, where most of the particles reside in a single fragment. The approximations for  $\xi$  improve for larger systems when Coulomb is ignored but become worse for large systems when Coulomb is included. This arises because a large system does not wish to form a single drop when Coulomb is included.

At high temperatures the sub-Poissonian behavior may be roughly understood as arising from particle conservation. As seen in section II when considering binomial distributions, one expects a negative correlation of order  $1/N$ , where  $N$  is the maximum number of IMFs that fit into the system.

The super-Poissonian (or nearly super-Poissonian when Coulomb is included) behavior at the fragmentation threshold is especially interesting. Perhaps, this may be understood by stating that the partition function is sampling two competing configurations, one with one large fragment surrounded by gas and a second one where numerous IMFs are present. At the fragmentation threshold, where the system is undergoing a transition, both configurations occur leading to a broadened multiplicity distribution. Figure 3 displays  $\xi$ , again scaled by  $A$ , as a function of temperatures between 7 and 9 MeV, for 3 sizes,  $A = 250$ ,  $A = 500$  and  $A = 1000$ . Coulomb is ignored in these calculations. As the system size increases a singularity in  $\xi$  develops at the boiling temperature. This is related to a discontinuity in the energy vs. temperature at constant volume [19], which is characteristic of this model but not characteristic of a typical liquid-gas transition. In a liquid-gas transition  $C_p$  becomes singular but not  $C_V$ . Since the peak in  $\xi$  vs.  $T$  is linked to the discontinuity in the energy density at the same temperature, the peak might disappear in a microcanonical treatment.

The multiplicity distributions for the  $A = 250$  system with Coulomb ignored are shown in Figure 4 for three temperatures, 7, 8 and 9 MeV. They are compared to negative binomial and binomial distributions respectively, where the two parameters are chosen to fit the mean and variance of the distributions. At 7 and 9 MeV, the two-parameter fits seem quite sufficient to describe the multiplicity distributions, whereas at 8 MeV, where the distribution is strongly super-Poissonian, the distribution's shape is poorly described by a negative binomial fit. This emphasizes that two classes of events, corresponding to the two phases, contribute at this temperature.

## V. COMPARISON WITH THE PERCOLATION MODEL

Here, we present a brief comparison of the results of the canonical model described in the previous sections with a percolation calculation [5]. For the percolation calculation, a cubic lattice of sites within a specified radius of the center are attached by bonds. The bonds are then broken with a probability  $p$ . When  $p$  is in the neighborhood of  $p_c = 0.7512$ , the system undergoes a second order phase transition and the size of the average largest cluster rapidly falls.

In the process of comparing percolation calculations to nuclear data, Li et al. [20] have developed a simple mapping of the bond breaking probability with the temperature. By using this mapping we are able to plot the results against temperature instead of  $p$ , and more readily compare to the results of the statistical model presented earlier. In the calculation presented here, the number sites in the spherical lattice was 203 and an IMF is defined as a fragment with mass between 6 and 40.

The mean IMF multiplicity and correlation coefficients are displayed in Figure 5. They are contrasted to the results of the canonical-ensemble calculations where  $A$  was chosen as 200 and Coulomb was ignored. There are three striking differences in the results. First, the percolation calculation does not yield as many fragments as the statistical calculation, which produces over twice as many fragments. Secondly, the percolation calculation does not exhibit a spike in the correlation coefficient as plotted against the temperature. This is expected as the percolation model does not contain a first order phase transition. Finally, the correlation coefficient is much larger for the case of the percolation calculation at low temperature. This is due to the fragmentative nature of percolation, where the existence of a fragment opens surface for the production of a second fragment [5].

## VI. MICROCANONICAL CALCULATIONS

A microcanonical approach, which considers configurations only at a specific energy, would be more realistic since nuclear collisions do not take place with contact to a heat bath. The importance of performing microcanonical calculations is emphasized by the existence of the first order phase transition, which collapses a wide range of energy densities to a narrow range of temperatures. In this section we present expressions for calculating fragmentation observables within a microcanonical context.

It is straightforward to obtain the needed microcanonical quantities from the expressions for partition functions by Fourier transforming corresponding canonical objects over a range of complex  $\beta \equiv 1/T$ . For instance, the level density,  $\rho(E)$ , may be obtained from the partition functions through,

$$\begin{aligned}\rho(E) &= \text{Tr}_\alpha \delta(E - E_\alpha) \\ &= \frac{1}{2\pi} \int d\beta \Omega_A(i\beta) e^{i\beta E}.\end{aligned}\tag{23}$$

One may calculate recursion relations for the factorial moments and for the multiplicity distributions at fixed energy. First we consider,  $f_{b,A,m}(i\beta)$  and  $p_{b,A,n}(i\beta)$  which are the canonical quantities without the normalization brought on by dividing by  $\Omega$ . As described in the appendix, they may be found via recursion relations.

$$\begin{aligned}f_{b,A,m}(\beta) &\equiv \Omega_A(\beta) F_{b,A,m}(\beta) \\ &= \sum_{k \in b} \omega_k f_{b,A-a_k,m-1}(\beta)\end{aligned}\tag{24}$$

$$\begin{aligned}p_{b,A,n}(\beta) &\equiv \Omega_A(\beta) p_{b,A,n}(\beta) \\ &= \frac{1}{n} \sum_{k \in b} \omega_k p_{b,A-a_k,n-1}(\beta)\end{aligned}\tag{25}$$

The factorial moments and multiplicity distributions at fixed energy  $E$  may then be expressed as,

$$\begin{aligned}F_{b,A,m}(E) &= \frac{\int d\beta f_{b,A,m}(i\beta) e^{i\beta E}}{2\pi \rho(E)} \\ P_{b,A,n}(E) &= \frac{\int d\beta p_{b,A,n}(i\beta) e^{i\beta E}}{2\pi \rho(E)}\end{aligned}\tag{26}$$

However, the integrations over  $\beta$  needed to obtain the relevant microcanonical quantities do make the calculations significantly more numerically intensive. It is not clear to what degree the stationary-phase approximation [21] might allow one to avert the numerically costly integration, especially given the first order phase transition which causes discontinuities as a function of  $\beta$ .

If one is interested in the microcanonical distribution, for a range of energies in the neighborhood of  $E$ , rather than for an exact value of  $E$ , one may replace the delta function in Eq. (23) by a Gaussian,

$$\delta(E - E_\alpha) \rightarrow \frac{1}{\sqrt{2\pi\eta^2}} \exp -\frac{(E - E_\alpha)^2}{2\eta^2},\tag{27}$$

where  $\eta$  defines the width of the neighborhood. One may incorporate the broadening of the  $\delta$  function by modifying the phase factors used in the Fourier transforms,

$$e^{i\beta E} \rightarrow e^{i\beta E} \exp -\frac{1}{2}\eta^2 \beta^2\tag{28}$$

Numerical implementation of the Fourier transform simplifies for broader widths  $\eta$ , as it effectively narrows the required integration range for  $\beta$ .

An alternative way to approach the constraint of energy conservation is to discretize the energy and measure it with integral values. One can then treat energy in the same manner with which one would treat other conserved charges. For instance, energy might be measured in steps of 0.1 MeV, with an integer  $Q$  measuring the energy. If  $\omega_i$  counts the number of states with energy  $q_i$  and mass  $a_i$ , the number of states of the system of mass  $A$  with net energy  $Q$  becomes,

$$N(A, Q) = \sum_{\langle \Sigma n_i a_i = A, \Sigma \langle n_i q_i = Q \rangle} \prod \frac{\omega_i^{n_i}}{n_i!} \quad (29)$$

One may then derive the recursion relation in a manner similar to the derivation of the recursion relation for the partition function shown in Section VIII A. Since there are two conserved “charges”, two recursion relations may be derived,

$$N(A, Q) = \sum_i \frac{a_i}{A} \omega_i N(A - a_i, Q - q_i) \quad (30)$$

$$= \sum_i \frac{q_i}{Q} \omega_i N(A - a_i, Q - q_i) \quad (31)$$

$$(32)$$

In a manner similar to the derivations in Sections VIII B and VIII D one may derive recursion relations for the factorial moments and multiplicity distributions,

$$F_{b,A,Q,m} = \sum_{k \in b} \omega_k F_{b,A-a_k,Z-Q_k,m-1} \frac{N(A - a_k, Q - q_k)}{N(A, Q)}, \quad (33)$$

$$P_{b,A,Q,m} = \sum_{k \in b} \omega_k \frac{1}{n} P_{b,A-A_k,Q-Q_k,n-1} \frac{N(A - a_k, Q - q_k)}{N(A, Q)}. \quad (34)$$

There are two practical differences between these expressions and the corresponding canonical expressions. First, an extra index has been added that denotes the energy of the system. Secondly, the index  $k$  refers to a set of states specified both by mass and charge. In practice this leads to a longer calculation by a factor of the number of energy steps squared. Thus if one wishes to perform a microcanonical calculation with an excitation energy of one GeV, using energy steps of 1.0 MeV, the required computer time would be expected to increase by  $10^6$  as compared to a microcanonical calculation at a single temperature.

## VII. CONCLUSIONS

The relations derived in this paper allow the exact calculation of all fragmentation observables within the context of a canonical ensemble of fragments. The relations allow the exact summation over all possible partitions of  $A$  nucleons within a fraction of a second of CPU time. The drawback of this approach is that interactions between fragments may only be included in a mean-field context, or through excluded volume. The advantage of this type of approach goes beyond numerical convenience. Unlike many Monte Carlo approaches, this technique has no arbitrary choices inherent to the algorithm. Thus, when one has finished with a calculation, one can more clearly state what expressions one has solved.

This approach can be made more realistic in three ways. First, the sum over intrinsic states, which here was performed in a liquid-drop context, can be replaced by a sum over true nuclear states without a significant cost in the time of the calculation. Secondly, isospin conservation may be included. It is straightforward to extend the recursion relations to two conserved charges [22] without significantly increasing the complexity of the approach. Finally, a microcanonical ensemble would represent a significantly more realistic description. Given that an entire region of energy densities is described by a single temperature, the spikes observed in our calculations of the correlation coefficient, and in previous calculations [22] of  $C_V$ , are expected to disappear in a microcanonical approach. As discussed in the previous section, the methods presented here might be extended to a microcanonical description, although computational pitfalls may complicate numerical implementation of the expressions derived here.

We finish by stating our belief that, although this type of approach is not yet to the stage where it can seriously be compared to data, this represents a revolution in the manner in which statistical physics can be applied to predicting observables for finite systems. We foresee that this approach will soon be developed to the stage where it can more conveniently, and more transparently, provide insight into the interpretation of a variety of experimental measurements.

## VIII. APPENDIX: DERIVATION OF RECURSIONS RELATIONS USED IN CANONICAL ENSEMBLES

### A. Recursion relation for the partition function

The recursion relation described here was first presented by Lee and Mekjian [23], and was first applied in a liquid-drop context by Chase and Mekjian [18].

The general relation for the partition function of non-interacting species is

$$\Omega_A = \sum_{\langle \sum n_k a_k = A \rangle} \prod_k \frac{\omega_k^{n_k}}{n_k!}, \quad (35)$$

where  $\omega_k$  is the partition function for a single particle of the species  $k$  which has size  $a_k$ . For each term in the sum, one can factor a term  $\omega_k$  out of the partition function. By using the fact that  $\sum n_k a_k / A = 1$ , one may rewrite the partition function,

$$\Omega_A = \sum_k \sum_{\langle \sum n_i a_i = A \rangle} \frac{n_k a_k \omega_k^{n_k}}{A n_k!} \prod_{i \neq k} \frac{\omega_i^{n_i}}{n_i!} \quad (36)$$

$$= \sum_k \omega_k \frac{a_k}{A} \sum_{\langle \sum n_i a_i = A - a_k \rangle} \prod_i \frac{\omega_i^{n_i}}{n_i!} \quad (37)$$

From combining this expression with Eq. (35), one can extract the recursion relation,

$$\Omega_A = \sum_k \omega_k \frac{a_k}{A} \Omega_{A - a_k}. \quad (38)$$

### B. The recursion relation for factorial moments

Factorial moments allow convenient calculation of the multiplicity distribution as seen in the subsequent subsection. Given the partition function,  $\Omega_A$ , the moments,  $F_{k,A,m}$ , are trivial to calculate for an individual species,  $k$ .

$$\begin{aligned} F_{k,A,m} &\equiv \langle n_k(n_k - 1)(n_k - 2) \cdots (n_k - m + 1) \rangle \\ &= \frac{1}{\Omega_A} \sum_{\langle \sum n_i a_i = A \rangle} n_k(n_k - 1) \cdots (n_k - m + 1) \prod_i \frac{\omega_i^{n_i}}{n_i!} \\ &= \omega_k^n \frac{\Omega_{A - m a_k}}{\Omega_A}. \end{aligned} \quad (39)$$

However, they are more difficult to obtain when they are defined in terms of  $n_b$  comprised of several species with different masses,

$$n_b = \sum_{k \in b} n_k \quad (40)$$

However in this case one may proceed with the help of a recursion relation for the factorial moments. To derive the recursion relation, we consider the function  $f$ .

$$f_{A,m}(b) \equiv \sum_{\langle \sum n_k = A \rangle} \prod_k \frac{\omega_k^{n_k}}{n_k!} n_b(n_b - 1) \cdots (n_b - m + 1) \quad (41)$$

$$F_{b,A,n} = \frac{f_{A,n}(b)}{\Omega_A} \quad (42)$$

For the first term  $n_b = \sum_{k \in b} n_k$  in the sequence of  $m$  terms  $n_b(n_b - 1) \cdots (n_b - m + 1)$ , each power of  $n_k$  may be used to cancel  $n_k$  in the factorial. By then factoring  $\omega_k$  outside the sum over configurations, one may rewrite  $f$  as

$$f_{A,m}(b) = \sum_{k \in b} \omega_k \sum_{\langle \sum n_{k'} = A - a_{k'} \rangle} \prod_{k'} \frac{\omega_{k'}^{n_{k'}}}{n_{k'}!} n'_b(n'_b - 1)(n'_b - 2) \cdots (n'_b - m), \quad (43)$$



where  $n'_b$  represents the number of  $b$ -type fragments in the set  $k'$ , which differs from the previous set by the reduction of one fragment of type  $k$ . From the definition of  $f$ , one may rewrite Eq. (43),

$$f_{A,m}(b) = \sum_{k \in b} \omega_k f_{A-a_k, m-1}, \quad (44)$$

which leads to the recursive expression for  $F$ ,

$$F_{b,A,m} = \sum_{k \in b} \omega_k F_{b,A-a_k, m-1} \frac{\Omega_{A-a_k}}{\Omega_A}, \quad (45)$$

This recursion relation allows one to calculate factorial moments of increasing order and for increasingly large nuclei given knowledge of the partition function.

### C. Obtaining the multiplicity distribution from the factorial moments

One can express the multiplicity distribution  $P_{b,A,n}$  in terms of the factorial moments. Here,  $P_{b,A,n}$  is the probability of observing  $n$  fragments of type  $b$  in an event from a system of mass  $A$ . The desired expression, which we derive further below, has the simple form,

$$P_{b,A,n} = \sum_{m \geq n} F_{b,A,m} \frac{1}{(m-n)!n!} (-)^{m-n}, \quad (46)$$

where  $F_{b,A,m} = \langle n_b(n_b-1) \cdots (n_b-m+1) \rangle$ . Only factorial moments of order  $n$  or greater contribute to  $P_{b,A,n}$  since events with multiplicity  $n_b < m$  do not contribute to  $F_{b,A,m}$ .

To prove Eq. (46) we rewrite the right-hand side of Eq. (46) using the definition of factorial moments,

$$\begin{aligned} \sum_{m \geq n} F_{b,A,m} \frac{1}{(m-n)!n!} (-)^{m-n} &= \sum_{m \geq n} \sum_{\ell \geq m} P_{b,A,\ell} \frac{\ell!}{(\ell-m)!} \frac{1}{(m-n)!n!} (-)^{m-n} \\ &= \sum_{\ell \geq n} \sum_{m=0}^{\ell-n} P_{b,A,\ell} \frac{\ell!}{(\ell-n-m)!} \frac{1}{m!n!} (-)^m, \end{aligned} \quad (47)$$

where, in practice, the sums do not extend to  $\infty$  due to the finite size of the system. The sum over  $m$  can now be eliminated by using the identity,

$$\sum_{m=0}^k \frac{k!}{(k-m)!m!} (-)^m = (1-1)^k = \delta_{k,0}, \quad (48)$$

to obtain Eq. (46). Although Eq. (46) is easy to implement numerically, it is susceptible to problems with numerical accuracy due to the alternating signs. Our experience is that such problems set in when the multiplicities approach or exceed ten. However, a recursion relation for the multiplicity distribution, which is derived in the next section, allows calculation of the multiplicity distribution without first calculating the moments. Such an expression does not have alternating signs and therefore is less susceptible to numerical problems.

### D. The recursion relation for the multiplicity distribution

In the previous sections of the appendix, relations have been derived that give a recursion relation for the factorial moments, and also give the multiplicity distribution in terms of the factorial moments. In this section we derive a recursion relation for the multiplicity distribution, that will allow the calculation of the multiplicity distribution without first calculating the moments.

By inserting the recursion relation for factorial moments, Eq. (45), into the formula for deriving the multiplicity distribution in terms of factorial moments, Eq. (46), one obtains,

$$\begin{aligned}
P_{b,A,n} &= \sum_{m \geq n} \frac{1}{(m-n)!n!} (-)^{m-n} \sum_{k \in b} \omega_k F_{b,A-a_k,m-1} \frac{\Omega_{A-a_k}}{\Omega_A} \\
&= \sum_{k \in b} \omega_k \frac{\Omega_{A-a_k}}{\Omega_A} \sum_{m \geq 0} \frac{1}{m!n!} (-)^m F_{b,A-a_k,n+m-1}
\end{aligned} \tag{49}$$

By replacing  $F_{b,A-a_k,n+m-1}$  in the above expression with its definition in terms of the multiplicity distribution,

$$\begin{aligned}
P_{b,A,n} &= \sum_{k \in b} \omega_k \frac{\Omega_{A-a_k}}{\Omega_A} \sum_{m \geq 0} \frac{1}{m!n!} (-)^m \sum_{m' \geq 0} P_{b,A-a_k,n+m+m'-1} \frac{(n+m+m'-1)!}{m'!} \\
&= \sum_{k \in b} \omega_k \frac{\Omega_{A-a_k}}{\Omega_A} \sum_{M \geq 0} P_{b,A-a_k,n+M-1} \frac{(n+M-1)!}{n!} \sum_{0 \leq m \leq M} (-)^m \frac{1}{m!(M-m)!} \\
&= \sum_{k \in b} \omega_k \frac{\Omega_{A-a_k}}{\Omega_A} P_{b,A-a_k,n-1} \frac{1}{n},
\end{aligned} \tag{50}$$

where the last step utilized the identity, Eq. (48).

In practice, the multiplicity distributions are calculated for small  $A$ , then for successively larger  $A$  using the recursion relation above. However, calculation of the  $n = 0$  term can not be determined from the recursion relation and must be determined through the constraint,  $\sum_n P_n = 1$ .

#### ACKNOWLEDGMENTS

This work was supported by the National Science Foundation, grant PHY-96-05207.

- [1] W. Bauer, Phys. Lett. B **150**, 53 (1985).  
W. Bauer, *et al.*, Nucl. Phys. A **452**, 699 (1986).  
W. Bauer, Phys. Rev. C **38**, 1297 (1986).  
W. Bauer and A. Botvina, Phys. Rev. C **52**, R1760 (1995).
- [2] X. Campi, J. Phys. A **19**, L917 (1986).  
Phys. Lett. **B208**, 351 (1988).
- [3] J.Pan and S. Das Gupta, Phys. Rev **C51**,1384(1995)
- [4] W.A. Friedman, Phys. Rev. **C42**, 667 (1990).
- [5] T. Gharib, W. Bauer and S. Pratt, to appear in Phys. Lett. B.
- [6] P. Chomaz, Ann. Phys. France **21**, 669 (1996).  
G.F. Burgio, Ph. Chomaz and J. Randrup, Phys. Rev. Lett. **69**, 885 (1992).
- [7] H. Feldmeier and J. Schnack, Prog. Particle Nucl. Phys. **39**, 393 (1997).
- [8] A. Ohnishi and J. Randrup, Phys. Lett. B **394**, 260
- [9] D. Kiderlen and P. Danielewicz, Nucl. Phys. A **620**, 346 (1997).
- [10] S. Pratt, C. Montoya and F. Ronning, Phys. Lett. **B349**, 261 (1995).
- [11] J. Randrup and S. Koonin, Nucl. Phys. A **356**, 321 (1981).
- [12] D.H.E. Gross, Rep. Prog. Phys. **53**, 605 (1990).  
J.P. Bondorf, A.S. Botvina, A.S. Iljinov, I.N. Mishustin and K. Sneppen, Physics Reports **257**, 133-221 (1995).
- [13] L.G. Moretto, *et al.*, Phys. Rev. Lett. **74**, 1530 (1995).  
L.G. Moretto, *et al.*, Phys. Rep. **287**, 249 (1997).
- [14] J. Toke, D.K. Agnihotri, B. Djerroud, W. Skulski and W.U. Schroeder, Phys. Rev. C **56**, R1686 (1997).
- [15] M.B. Tsang and P. Danielewicz, Phys. Rev. Lett. **80**, 1178 (1998).
- [16] W. Bauer and S. Pratt, LANL report nucl-th/9809024 (1998).
- [17] L.G. Moretto, L. Bealieu, L. Phair, and G.J. Wozniak, Los Alamos report, nucl-ex/9709001 (1997).
- [18] K.C. Chase and A.Z. Mekjian, Phys. Rev **C52**,R2339(1995)
- [19] S. Das Gupta and A.Z. Mekjian, Phys. Rev **C57**,1361(1998).
- [20] T. Li, *et al.*, Phys. Rev. **C49**, 1630 (1994).

- [21] A. Bohr and B.R. Mottleson, Nuclear Structure, Vol. 1, World Scientific (1998).
- [22] S. Dasgupta, A. Majumder, S. Pratt and A. Mekjian, submitted to Physical Review C.
- [23] S.J. Lee and A.Z. Mekjian, Phys. Rev. C**47**, 2266 (1993).  
S.J. Lee and A.Z. Mekjian, Phys. Rev. C**45**, 1284 (1992).  
S.J. Lee and A.Z. Mekjian, Phys. Rev. C**50**, 3025 (1994).

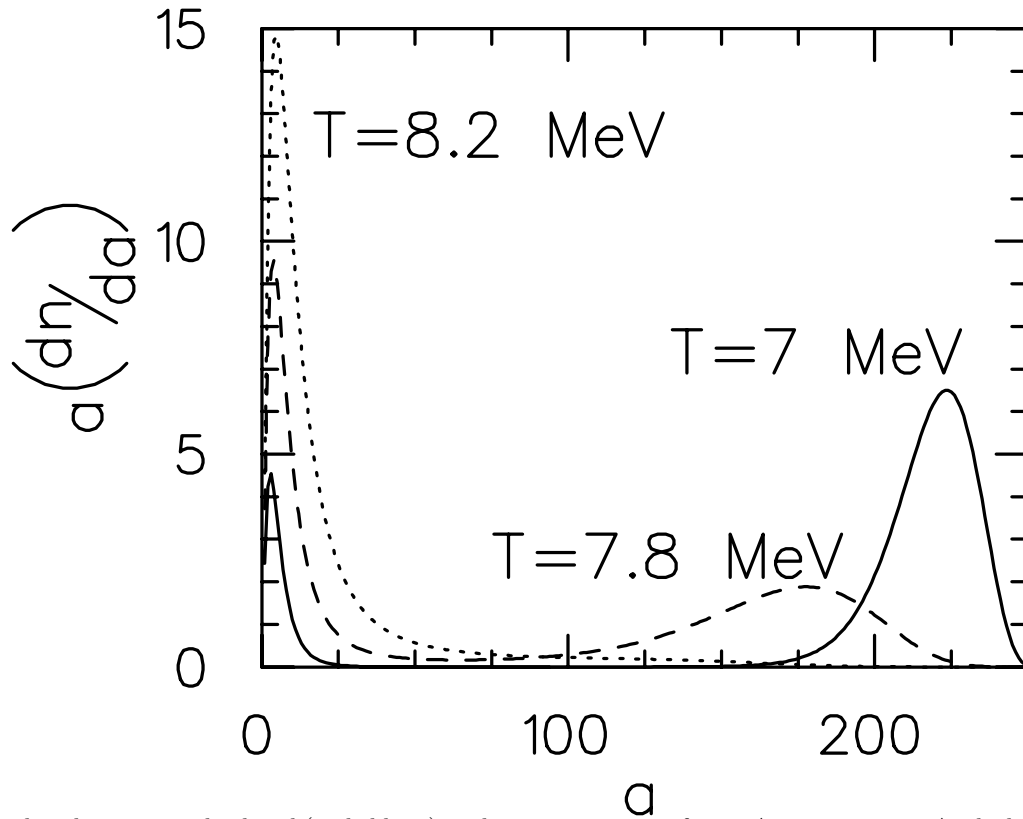


FIG. 1. Mass distributions are displayed (scaled by  $a$ ) at three temperatures for an  $A = 250$  system. At the high temperature, 8.2 MeV, (dotted line) the distribution is dominated by small fragments, while below the fragmentation threshold, at 7 MeV, (solid line), most nucleons reside in one fragment. At 7.8 MeV (dashed line), the system seems equally divided between the large cluster and small clusters. The transition occurs over a remarkably narrow range of temperatures.

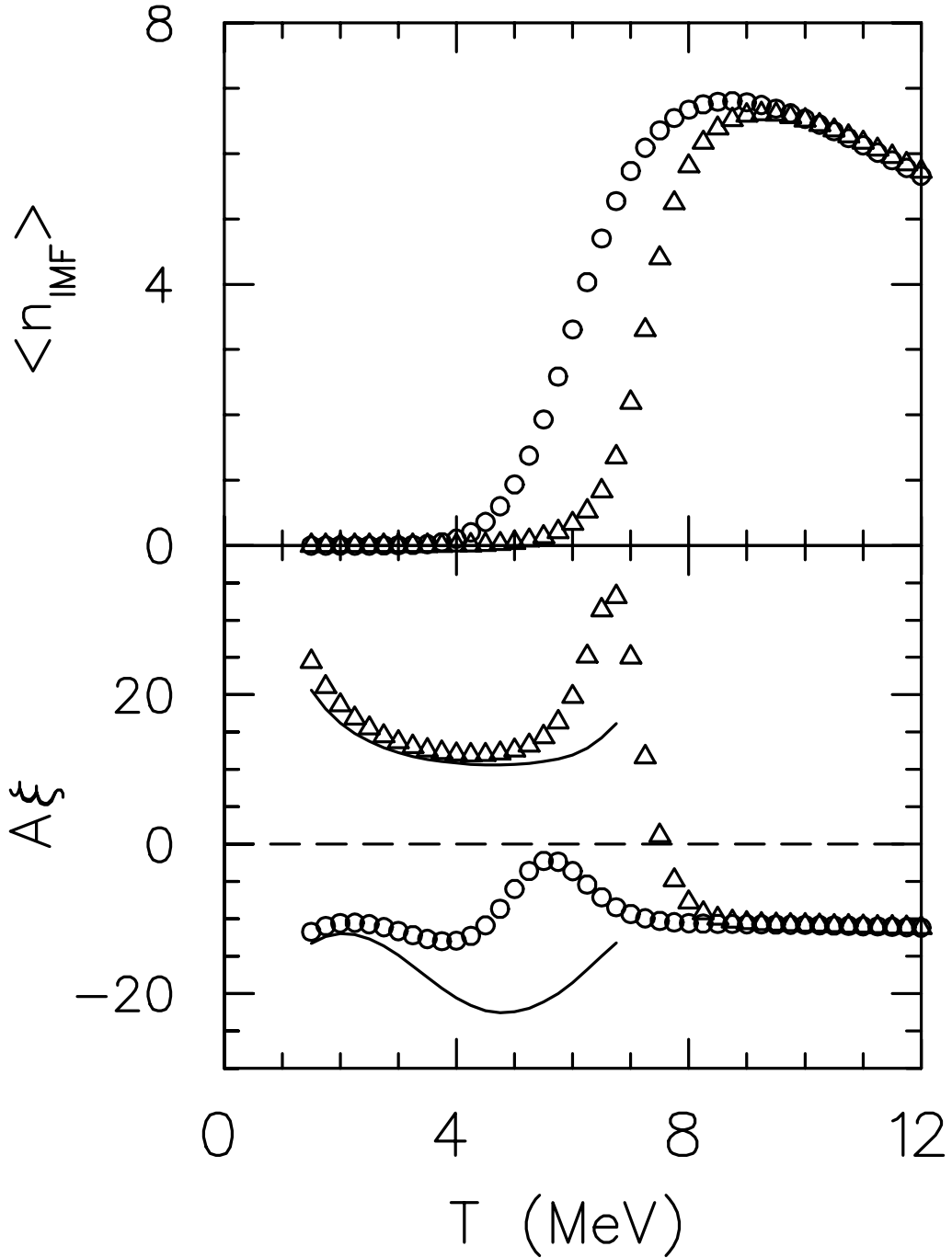


FIG. 2. The average multiplicity of IMFs, those fragments with masses from 6 to 40, are shown in the upper panel as a function of temperature for an  $A = 100$  system. Including Coulomb (circles) lowers the threshold temperature for fragmentation compared to when Coulomb is ignored (triangles). Correlation coefficients are displayed in the lower panel. The approximations described in the text, which are represented by lines, describe the behavior at low excitation. A positive correlation at the fragmentation threshold arises from two classes of events, those with and without a large cluster, both contributing at the fragmentation threshold.

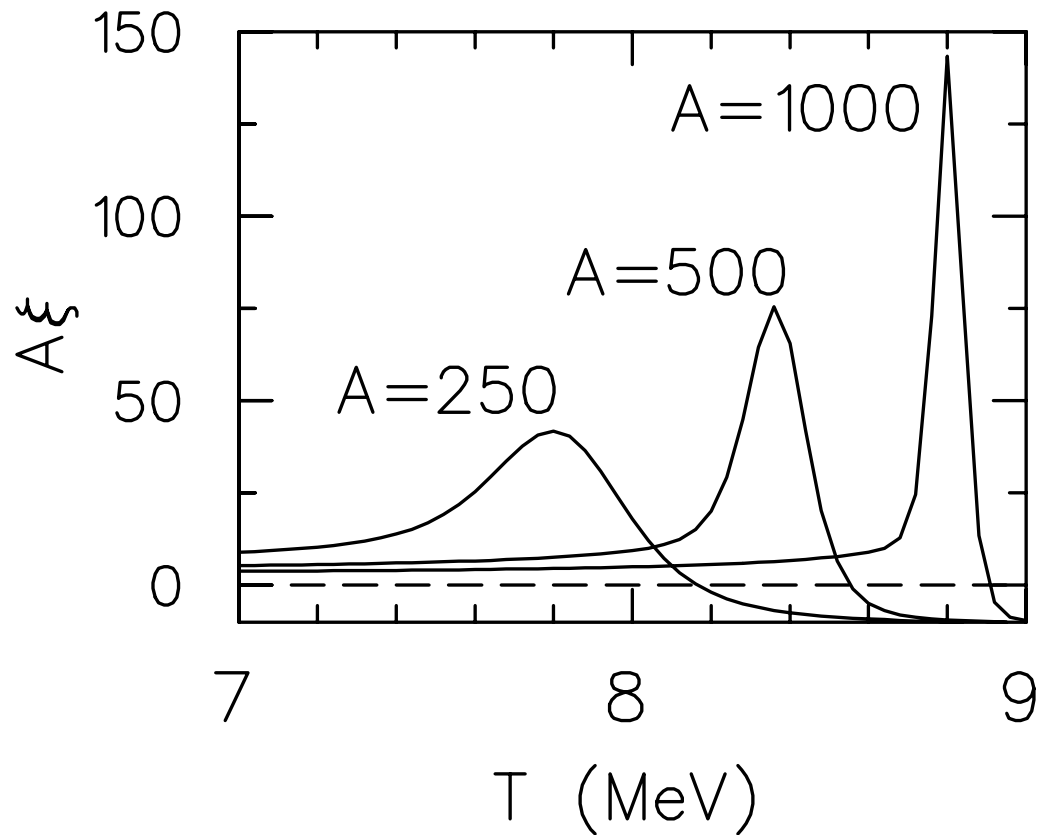


FIG. 3. The evolution of the correlation coefficient is shown for a small range of temperatures for increasing large system sizes. For large systems the peak narrows into a singularity, a signal of discontinuous behavior. This is remarkable given that it is the volume, not the pressure, that is held constant while the temperature is changed. Coulomb has been neglected in this calculation.

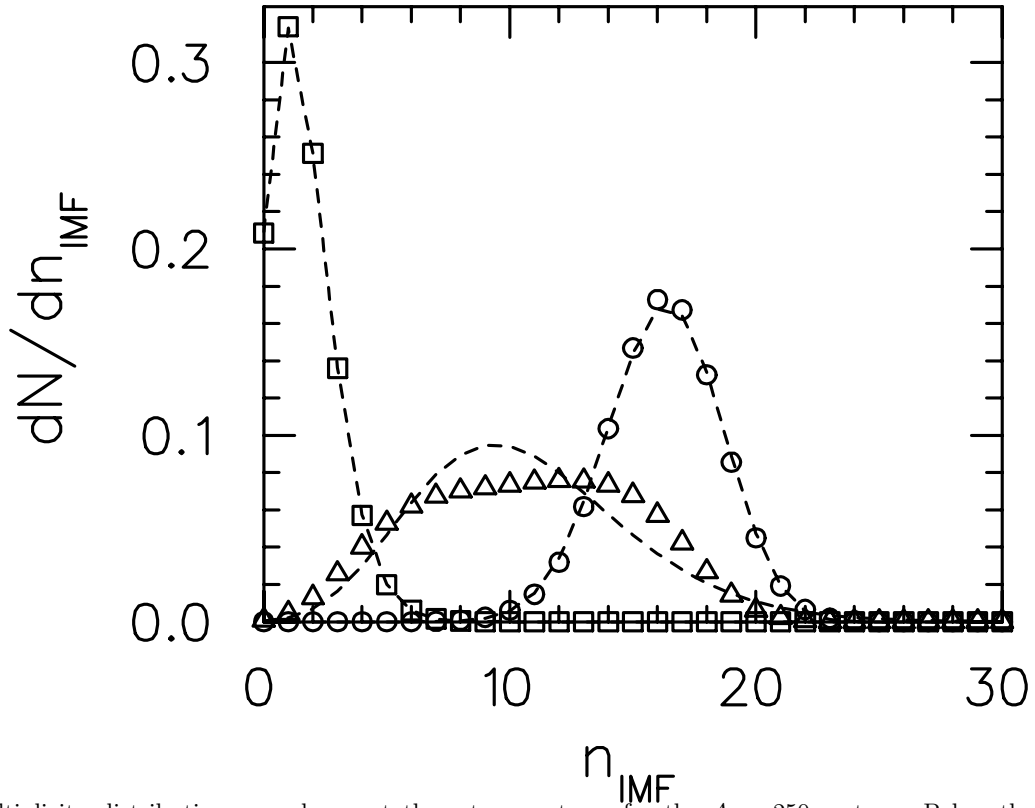


FIG. 4. Multiplicity distributions are shown at three temperatures for the  $A = 250$  system. Below the fragmentation threshold at a temperature of 7 MeV (squares), the distribution is peaked at a low multiplicity and is well described by a negative binomial distribution shown as a dashed line. At a high temperature of 9 MeV (circles), the distribution is sub-Poissonian and well described by the binomial distribution (dashed line). At 8 MeV (triangles), the multiplicity distribution is strongly super-Poissonian and is not even well described by a negative binomial.

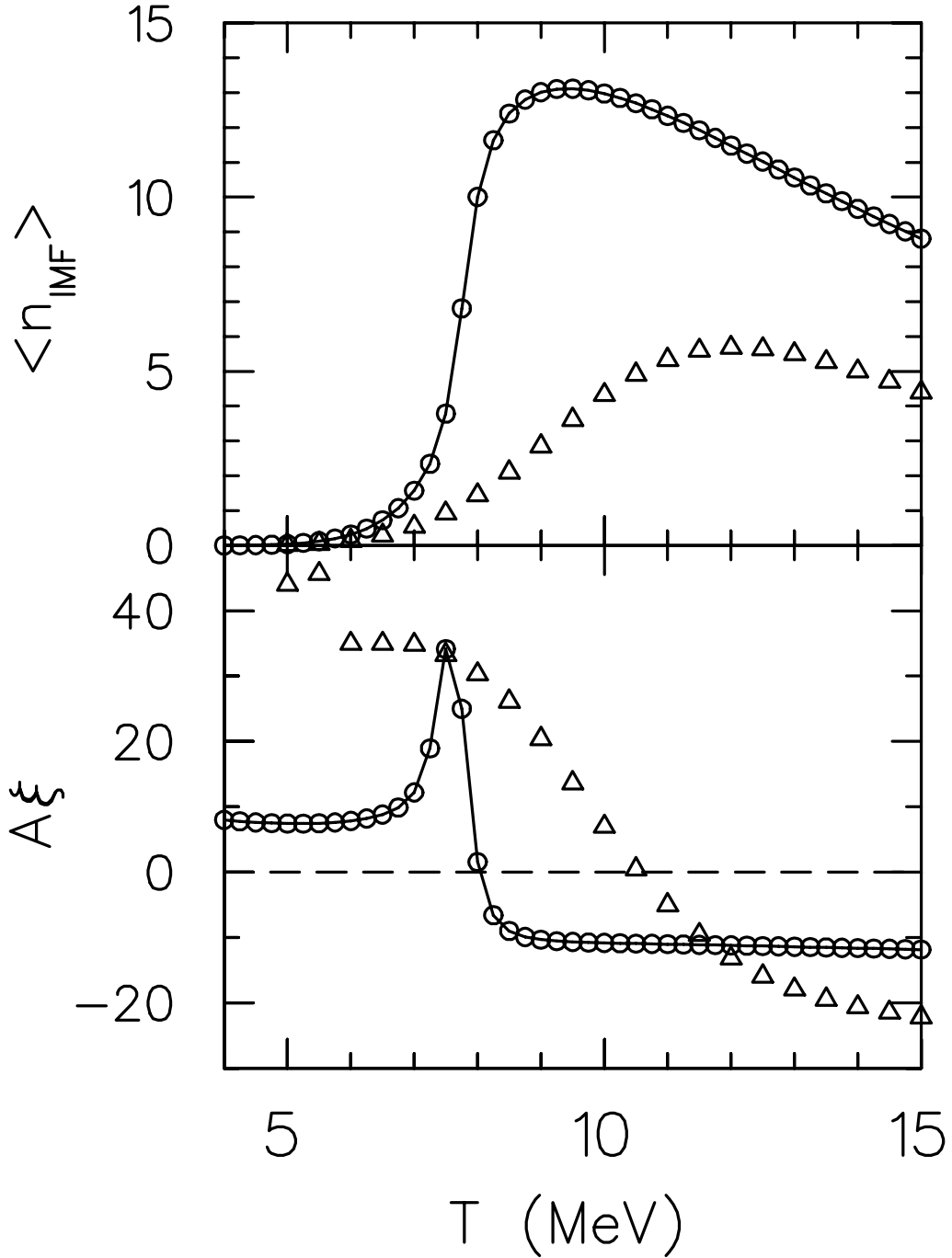


FIG. 5. IMF multiplicity distributions are displayed in the upper panel, while correlation coefficients are displayed in the lower panel. Percolation calculations, based on a spherical lattice of 203 sites are represented by triangles while the canonical ensemble, with  $A = 200$  and no Coulomb effects, is represented by circles. The percolation model does not exhibit a first order phase transition, hence it's correlation coefficient does not show a spike at the critical temperature. Other notable differences are that the multiplicity in the statistical calculation reaches higher values than in the percolation model while the correlation coefficient in the percolation calculation reaches larger values at low temperatures.